Journal of Science and Transport Technology
Journal homepage: https://jstt.vn/index.php/en

Removal of phosphate from activated biochar prepared from bentonite biochar composite: Kinetic, equilibrium, thermodynamic adsorption

Ta Thi Hoai[1], Nguyen Thi Hai[1,*], Minh Trang Hoang[1], Nguyen Thi Hoang Ha[2], Thao Hoang-Minh[2]
[1]VNU University of Science, Vietnam National University, Hanoi, 334 Nguyen Trai, Thanh Xuan, Hanoi, Vietnam
[2]Vietnam Japan University, Vietnam National University, Hanoi, Luu Huu Phuoc, Tu Liem, Hanoi, Vietnam

Article info
Type of article:
Original research paper

DOI:
https://doi.org/10.58845/jstt.utt.2026.en.6.3.77-92

***Corresponding author:**
Email address:
nguyenthihai128@hus.edu.vn

Received: 20/06/2025
Received in Revised Form: 26/05/2026
Accepted: 01/07/2026

Abstract: Excess phosphorus threatens both aquatic ecosystems and human health. This study investigated the kinetic, equilibrium, and thermodynamic behavior of phosphate (PO_4^{3-}) adsorption using a low-cost composite adsorbent synthesized from bentonite and rice-husk–derived activated carbon. Batch experiments examined the influence of initial PO_4^{3-} concentration, temperatures, contact time, pH, and co-existing anions. The findings revealed that the PO_4^{3-} adsorption onto synthesized material was best represented by Langmuir isotherm theory. Kinetic analyses showed that PO_4^{3-} adsorption follows both pseudo-first and pseudo-second-order models, exhibiting strong correlation coefficients ($R^2 = 0.99$). The optimal pH for adsorption was identified as 7. The presence of co-existing anions such as CO_3^{2-}, SO_4^{2-}, and Cl^- notably decreased the efficiency of PO_4^{3-} removal. The synthesis of material based on bentonite and biochar from rice husk demonstrates strong potential for PO_4^{3-} removal and recovery from water.

Keywords: Phosphate, adsorption, activated biochar, bentonite biochar composite, thermodynamic, water environment.

1. Introduction

Phosphorus serves as a crucial growth-limiting factor in plant development. However, when the concentration of phosphorus in cultivated soil surpasses a certain threshold, it can impede the absorption of other essential micronutrients, particularly iron and zinc [1, 2]. Furthermore, elevated levels of phosphorus and nitrogen in aquatic systems can lead to an increase in algal blooms and aquatic plant proliferation, which may result in eutrophication [3]. This phenomenon markedly depletes the level of dissolved oxygen in water, which has a negative impact on aquatic ecosystem and diminishing the aesthetic value of impacted water bodies. Consequently, it is imperative to control eutrophication by mitigating the anthropogenic introduction of phosphorus into surface waters.

The main route for anthropogenically phosphorus to enter the surface water is via discharging of wastewater, thus many researches have focused on its removal using various approaches, such as enhanced biological uptake [4], adsorption [5], ion exchange [6], and chemical

precipitation [7]. Among the various methodologies, adsorption is recognized as a particularly advantageous approach. This method is characterized by its operational simplicity, straightforward design, high selectivity, and effective capacity for the removal of PO_4^{3-}, even at low concentrations. Additionally, the process generates minimal by-products, which enhances its overall sustainability [8, 9]. In addition, a wide range of low-cost adsorbent were utilized, the ability of regenerating and recycling the used adsorbent, and the possibility of recovering adsorbate make the adsorption even more preferrable for removing of PO_4^{3-} [10]. The recovered and recycled PO_4^{3-} from wastewater can be utilized in a variety of ways, including making agricultural fertilizer [10, 11]. To further encourage the use of adsorption for the removal and recovery of PO_4^{3-} from wastewater, it is necessary to identify a material that is inexpensive and widely accessible in the local area.

Clays are increasingly used as low-cost, widely available adsorbents for wastewater treatment because of their strong adsorption properties. Natural clays such as bentonite, zeolite, and kaolin have widely been studied for removing pollutants [10, 12]. Among them, with bentonite being especially favored for its effectiveness removal cationic contaminants, environmental friendliness, and high recyclability [13, 14]. However, the original bentonite appears to have poor selectivity and adsorption capacity for anionic contaminants, which limits the material's use in a number of specific circumstances.

Biochars are carbon-rich materials produced by pyrolyzing various types of biomass under limited oxygen conditions [10]. In water treatment applications, biochars are considered a promising adsorbent because they require fewer chemicals and simpler procedures for production, while achieving comparable adsorption capacities to activated carbons [15, 16]. Their large surface area, porous structure, and profusion of oxygen functional groups provide them the ability to adsorb substances [15]. Additionally, biochars have proven beneficial for soil remediation, as they can enhance soil fertility and improve soil structure. Furthermore, producing biochars from biomass helps reduce greenhouse gas emissions from open burning and promotes circular economic agricultural practices.

A material synthesized from bentonite and rice husk, as described in our previous investigations by Hoang-Minh et al. [17], demonstrated a good adsorption capacity for ammonium. To further evaluate its potential for multi-contaminant treatment, the current study investigates the adsorption performance of this bentonite-rice husk composite concerning PO_4^{3-}. The study meticulously examines the kinetics, equilibrium, and thermodynamics of the BRK material for the adsorption of PO_4^{3-} from water. his analysis aims to elucidate the adsorption behavior, efficiency, and underlying mechanisms. Kinetic models are employed to assess the rate of adsorption and the equilibrium-achieving time. Equilibrium studies aim to calculate the maximum adsorption capacity and to characterize the interactions between PO_4^{3-} ions and the adsorbent. Thermodynamic analysis is conducted to evaluate the spontaneity and feasibility of the adsorption reaction. Additionally, an effect of co-existing anions was investigated to determine their possible influence on the PO_4^{3-} removal effectiveness of the material. The findings of this study are expected to support the development of low-cost, efficient materials for multi-pollutant removal from contaminated water.

2. Materials and methods

2.1. Adsorbent preparation

Bentonite was collected from a bentonite mine in Di Linh district, Lam Dong province, Vietnam. The raw bentonite was then milled and sieved to obtain particles less than 40 μm. Rice husk (RH) was collected in Hanoi, Vietnam, washed, and dried at 80 °C in an oven. After drying, the rice husk was ground and sieved to obtain particles between 0.5 and 1 mm.

The bentonite biochar composite (BRK) was prepared following a method reported in previous research [17]. A mixture of bentonite and rice husk at a 1:5 ratio was pyrolyzed at 400 °C for 3 hours and followed by the modifiaction with KOH 2M. The adsorbent was then rinsed with deionized water until the solution reached a pH of 7 and was subsequently dried at 80 °C for experiments. A simple screening test was conducted to compare the ability of raw rice husk, bentonite, and the composite material BRK to remove PO_4^{3-} from water. The experiment was performed with an adsorbent dose of 2 g/L, a contact time of 24 hours, a pH of 7.0, a temperature of 30 °C, and an initial PO_4^{3-} concentration of 3 mg/L. The results demonstrated that the adsorption capacities of the raw materials RH, bentonite, and BRK were 0.03, 0.06, and 0.13 mg/g, respectively. The significantly higher adsorption capacity of BRK compared to the unmodified rice husk and bentonite confirms that the modification process greatly enhanced adsorption performance. This improvement underscores the necessity and effectiveness of material modification in developing a more efficient adsorbent for PO_4^{3-} removal.

The characterization of pristine BRK was detailed in our previous study [17]. Briefly, BRK exhibits a highly porous, heterogeneous surface structure, with numerous holes and wide grooves that contribute to its large surface area and structural asymmetry. This porosity results from the presence of biochar and is further enhanced by chemical activation with KOH. SEM analysis also confirms the inclusion of bentonite, recognizable by its characteristic layered, plate-like morphology. EDX analysis shows that BRK is primarily composed of C, O, Si, K, Ca, and Fe, with a notably high potassium content, indicating successful KOH activation. FTIR spectra reveal functional groups such as –OH, C=O, C=C, and CO, which are typical of biochar, while the Si–O vibration near 1031 cm^{-1} confirms the presence of bentonite. Nitrogen adsorption–desorption measurements indicate a S_{BET} of 4.89 m^2/g and a pore volume of 0.009 cm^3/g, suggesting a highly accessible porous structure. Additionally, BRK exhibited a point of zero charge (pH_{PZC}) of 9.1.

In this study, after the adsorption process, the surface morphology and atomic composition of PO_4^{3-}-laden BRK were determined using SEM (Nano SEM FEI-450) integrated with EDX spectroscopy (TEAM Apollo XL-EDAX). The functional groups of PO_4^{3-}-laden BRK were analyzed using a Jasco FTIR-6300 spectrometer.

2.2. Adsorption experiment

A batch adsorption experiment of KOH-treated BRK toward PO_4^{3-} was conducted by adding 0.1 g of adsorbent to the Erlenmeyer flask contatining 50 mL of PO_4^{3-} solution at a target initial concentration. The blend was shaken at 160 rpm using a shaker. After filtration through glass paper, the PO_4^{3-} concentration in solution were measured using the Skalar method (SKALAR model 21,050,900, Netherlands).

The effect of initial pH solution on the removal efficiency of PO_4^{3-} with a 50 mL solution of 3 mg/L of PO_4^{3-}. The initial pH was adjusted from 2.0 to 11.0 using HNO_3 0.1M and NaOH 0.1M solutions. Three replicates were performed for all experiments. The adsorption efficiency (H %) in removal of PO_4^{3-} was determined by Eq. (1):

$$H\ (\%) = \frac{(C_o - Ct)}{C_o} \times 100\ (\%) \qquad (1)$$

where, C_o and C_t are the PO_4^{3-} concentrations before and after adsorption, respecitvely (mg/L).

The adsorption isotherms at 10, 30 and 50 °C were determined by contacting 0.1 g BRK with 50 mL of PO_4^{3-} solution (0–50 mg/L) for 24 hours at pH 7, under stirring conditions (160rpm). The adsorbed PO_4^{3-} amount (q_e) at equilibrium was calculated by Eq (2).

$$q_e = \frac{(C_0 - C_t) \times V}{m} \qquad (2)$$

where C_o and C_t are the PO_4^{3-} concentration before and after adsorption (mg/L), *V* is the solution volume (L), and m is the adsorbent's dry weight (g).

Three isotherm models, including Langmuir, Freundlich, and Redlich–Peterson were applied to

analyze the adsorption data. The nonlinear Langmuir equation was given in Eq. (3):

$$q_e = \frac{q_m K_L C_e}{1+K_L C_e} \quad (3)$$

where q_m (mg/g) is the maximum adsorption capacity of BRK, and K_L (L/mg) is the Langmuir constant associated with binding site affinity.

The Freundlich isotherm, an empirical model, is suitable for describing multilayer adsorption. The nonlinear Freundlich equation is defined by Eq. (4):

$$q_e = K_F(C_e)^{1/n} \quad (4)$$

where K_F ((mg/g)(L/mg)$^{1/n}$) and n present Freundlich constants.

The Redlich–Peterson isotherm incorporates features of both Langmuir and Freundlich theory, making it suitable for adsorption on homogeneous and heterogeneous surfaces. It is a three-parameter empirical model that provides a more flexible approach to fitting experimental data. The nonlinear Redlich–Peterson equation is expressed as follows (Eq. 5):

$$q_e = \frac{K_R C_e}{1+a_R C_e^{\beta}} \quad (5)$$

where K_R (L/g) and a_R ((L/mg)g) represent the Redlich–Peterson constants, and β represents an exponent with a value range from 0 to 1, representing the degree of heterogeneity of the adsorption process. When β = 1, the Redlich–Peterson model reduces to the Langmuir model; when β < 1, it resembles the Freundlich model. This model is beneficial for fitting experimental data over a wide concentration range where deviations from ideal Langmuir or Freundlich behavior may occur.

The adsorption kinetic tests were performed with 3 mg/L PO_4^{3-} solutions at pH 7. The solution was collected at desired time intervals, from 1 to 1440 min. Three adsorption kinetic models, including pseudo-first-order, pseudo-second-order, and intraparticle diffusion models, were applied to interpret the batch experiments data. The rate constant for PO_4^{3-} adsorption on adsorbent was determined by pseudo-first-order rate model equation (Eq. 6) given as follows:

$$q_t = q_e(1-e^{-k1t}) \quad (6)$$

where q_t (mg/g) represents the quantity of PO_4^{3-} adsorbed at time t (min), and k_1 (1/min) acts as the rate constant.

The equation of pseudo-second-order model (Eq. 7) is given below:

$$q_t = \frac{k_2 q_e^2 t}{1+ k_2 q_e t} \quad (7)$$

where k_2 (g/mg×min) refers to the model rate constant.

The intraparticle diffusion model is commonly used to describe the rate of diffusion of adsorbate molecules into the adsorbent's internal pores. The general form of the nonlinear intraparticle diffusion equation (Eq. 8) is given by:

$$q_t = K_{diff} t^{1/2} + C \quad (8)$$

where K_{diff} (g/mg × min$^{1/2}$) is the model rate constant, C (mg/g) is a constant reflecting the boundary layer effect or the intercept, representing the difference between the external mass transfer and the intra-particle diffusion steps.

The competitive effect of coexisting anions was studied by using three anions: Cl^-, SO_4^{2-}, CO_3^{2-}. These experiments were conducted by adding individual anionic ions into PO_4^{3-} solutions of 3 mg/L at different initial concentrations (0.01 and 0.1 M). The solution after equilibrium time was filtered to test the concentration of remaining PO_4^{3-}

3. Results and discussions

3.1. Analysis of adsorption isotherm and equilibrium

Fig. 1 and Table 1 present the non-linear fitting of PO_4^{3-} adsorption onto BRK using three commonly applied isotherm models, including Langmuir, Freundlich, and Redlich–Peterson. Among them, the Langmuir adsorption model consistently exhibited the highest correlation coefficients (R^2 = 0.95–0.96) and the lowest chi-square values (χ^2 = 0.007–0.012), which demonstrates the closest fit to the experimental data. This implies that on a homogenous surface with a small number of identical active sites, the

adsorption process mostly follows monolayer form, as described by Langmuir theory. The correlation coefficients (R^2) and lowest chi-square (χ^2) values of Redlich–Peterson model also demonstrated a good fit, particularly at lower temperatures, with behaviour approaching that of the Langmuir model, while the Freundlich model displayed relatively lower R^2 values and higher χ^2 values, pointing to less suitability for the system.

As shown in Table 1 and Fig. 1, the adsorption process was also strongly influenced by temperature. The maximum adsorption capacity of BRK toward PO_4^{3-} increased from 1.36 mg/g at 10 °C to 1.55 mg/g at 50 °C. A similar trend was reported by Liu et al. [18] who observed that the PO_4^{3-} adsorption performance on CaO-biochar composites prepared from eggshell and rice straw increased slightly with rising temperature. This trend indicates that PO_4^{3-} adsorption onto BRK is an endothermic process [18, 19]. The adsorption capacity of BRK increases with temperature, which can be attributed to the increased ion mobility, increased diffusion into interior pores, and higher contact with active sites.

These observations are consistent with previous studies on bentonite-derived adsorbent or biochar derived adsorbents such as modified bentonite with $Mg(OH)_2$ [20], bentonite modified and encapsulated in Ca-alginate beads [5], and CaO-biochar composites [18], all of which demonstrate similar temperature-dependent PO_4^{3-} adsorption behavior.

A comparison of the adsorption abilities between BRK and previously reported materials shows that BRK performs lower than most biochars (e.g., rice husk biochar [21], corn biochar [22]), modified biochars (e.g., Mg-modified corncob hydrochar [23], Fe- and Zr-loaded activated carbon nanofibers [24]), modified bentonites (e.g., Mg-modified bentonite [20], hydroxy-Fe–Al pillared bentonite [25]), and composite materials such as dolomite-doped biochar–bentonite [26] (Table 2). However, BRK remains comparable to, or even outperforms, several raw clay minerals [27]. The higher capacities reported for other materials are largely attributed to higher adsorbent dosages and initial pollutant concentrations. Moreover, the lower adsorption capacity of BRK compared to the modified materials can be attributed to the absence of metal modification, which typically increases the number of active sites and significantly enhances adsorption performance [28].

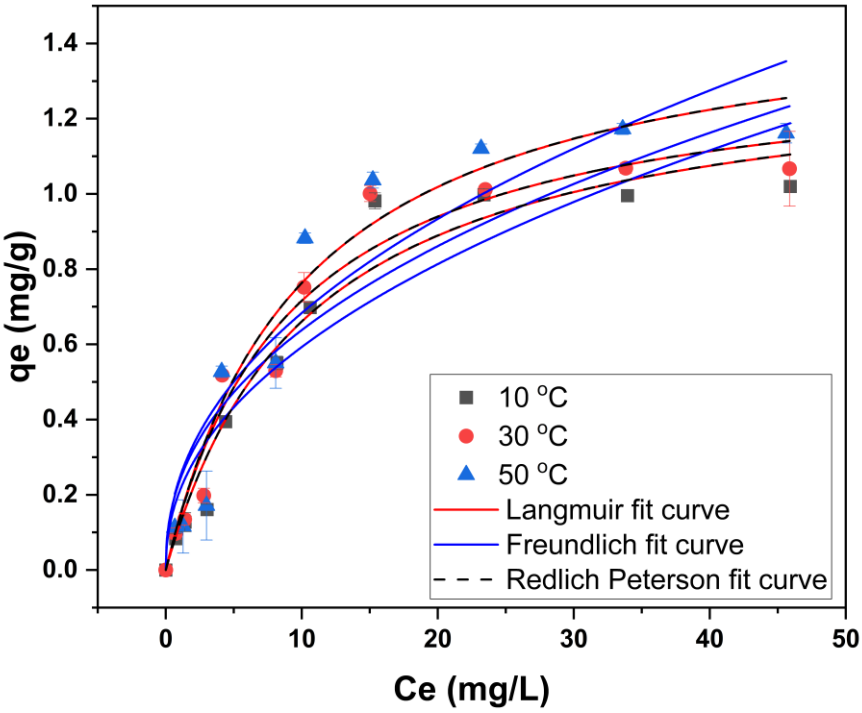

Fig. 1. Adsorption isotherm of PO_4^{3-} on BRK

Table 1. Parameters of nonlinear isotherm models for PO_4^{3-} adsorption on BRK.

Temperature	Parameters	10 °C	30 °C	50 °C
Langmuir	K_L (L/mg)	0.095 ± 0.023	0.110±0.026	0.100±0.027
	q_m (mg/g)	1.36±0.125	1.37± 0.113	1.55±0.155
	R^2	0.96	0.96	0.95
	χ^2	0.007	0.007	0.012
Freundlich	K_F ((mg/g)(L/mg)$^{1/n}$)	0.207±0.052	0.235±0.05	0.242±0.063
	n	0.455±0.07	0.433±0.075	0.450±0.08
	R^2	0.89	0.90	0.87
	χ^2	0.020	0.019	0.028
Redlich Peterson	K_{RP} (L/g)	0.129±0.052	0.150±0.057	0.152±0.07
	a_R ((L/mg) g)	0.095±0.139	0.110±0.141	0.099±0.16
	β	1±0.272	1±0.234	1±0.299
	R^2	0.95	0.95	0.93
	χ^2	0.008	0.008	0.0138

Table 2. Comparison of PO_4^{3-} adsorption capacity between BRK and reported materials

Materials	Experimental conditions				q_m (mg/g)	Ref.
	pH	Dosage (g/L)	Initial concentration (mg/L)	T (°C)		
BRK	7	2	0-50	50	1.55	This study
Rice husk biochar	7	12.5	25-159	25	8.09	[21]
Corn biochar	7.8	10	84-6400	30	225	[22]
Mg-modified corncob hydrochar		2.5	20-15000	45	89.6	[23]
Fe- and Zr-loaded activated carbon nanofiber	4	1	1.5-20	25	26.3	[24]
Montmorillonite	4.5	1	0.15-5	25	0.3	[27]
Raw bentonite Mg Modified bentonite	6	2	0.05-25	25	0.391 2.900	[20]
Mixed hydroxy-Fe-Al pillared bentonite	3	4	25-60		10.5	[25]
Dolomite-doped biochar and bentonite		2.6	100		66.2	[26]

Despite its lower PO_4^{3-} adsorption capacity, BRK demonstrated effective NH_4^+ removal, with capacities reaching up to 20.57 mg/g [17]. This highlights BRK as a promising material for the simultaneous removal of multiple pollutants. Moreover, its performance toward PO_4^{3-} can be further enhanced through future modification to improve adsorption efficiency.

3.2. Analysis of adsorption kinetic

As seen in Fig. 2, three models, includings pseudo-first-order, pseudo-second-order, and intraparticle diffusion, were used to assess the kinetics of PO_4^{3-} adsorption onto BRK. This analysis was designed to understand the adsorption mechanisms and rate-controlling steps of the uptake process. The adsorption experiments were conducted over a time range of 0 to 1440 minutes (24 hours), and the results shown that the efficiency of PO_4^{3-} removal by BRK is remarkably dependent on the contact time.

A quick adsorption rate was occurred during the initial phase (0–60 minutes), attributed to the high number of active sites on the outer layer of the BRK material's surface. As time progressed, the number of unoccupied active sites decreased, leading to a gradual slowdown in the adsorption rate. After 60 minutes, no significant increase in adsorption capacity was recorded, indicating that equilibrium had been reached. The driving force for mass transfer between both solid and liquid states decreased at this time because the adsorption sites were probably saturated.

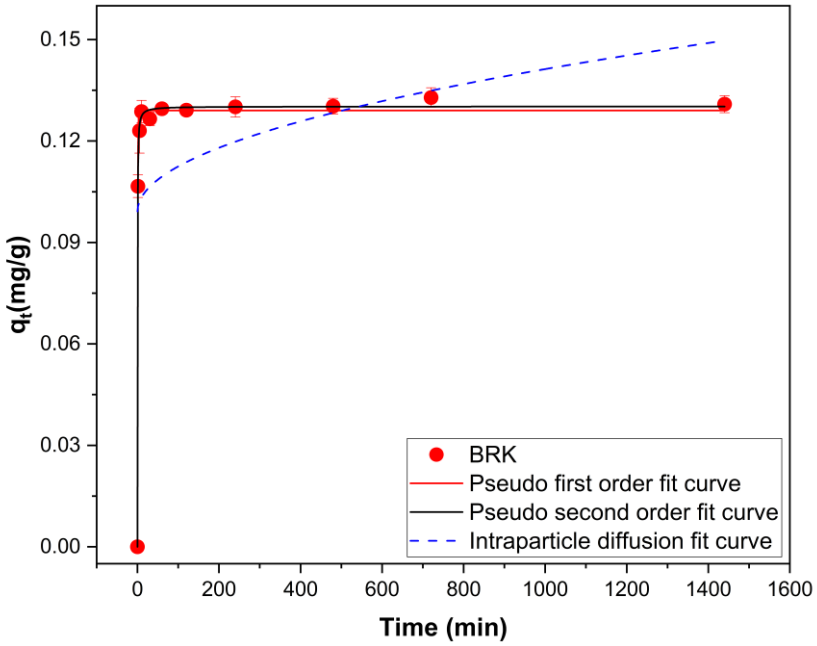

Fig. 2. Adsorption kinetic of PO_4^{3-} on BRK

Table 3. Nonlinear kinetic fitting parameters for PO_4^{3-} adsorption onto BRK

Models	Unit	BRK
q_{exp}	mg/g	0.13
Pseudo-first order		
q_e	mg/g	$0.129\pm8.8\times10^{-4}$
k_1	1/min	1.75±0.1227
R^2		0.99
χ^2		6.9×10^{-6}
Pseudo-second order		
q_e	mg/g	$0.130\pm5.3\times10^{-4}$
k_2	g/mg×min	34.08±2.791
R^2		0.99
χ^2		2.2×10-6
Intrapacticle diffusion		
K_{diff}	g/mg × $min^{1/2}$	$0.00133\pm9.6\times10^{-4}$
C	mg/g	0.099±0.016
R^2		0.176

The kinetic parameters for each model are summarized in Table 3. Among the three models analysed, the intraparticle diffusion model showed a poor fit, indicated by a low correlation coefficient (R^2 = 0.176). This implies that adsorption is not primarily driven by intraparticle diffusion. The intraparticle diffusion model's poor fit suggests that diffusion inside the particle pores does not regulate

the adsorption process.

In contrast, the experimental data was well-fitted by both the pseudo-first-order and pseudo-second-order models, with R^2 values close to 1.00 and very low chi-square values ($\chi^2 = 6.9\times10^{-6}$, $\chi^2 = 2.2\times10^{-6}$), These results indicate that these models accurately describe the kinetic of PO_4^{3-} adsorption on BRK. The equilibrium adsorption capacities, q_{eq}, from both models were found to be $0.129\pm8.8\times10^{-4}$ mg/g and $0.130\pm5.3\times 10^{-4}$ mg/g, respectively, which closely equal the experimental value of 0.13 mg/g.

The better fit of the pseudo-second-order model suggests that chemisorption may be the dominant mechanism at play, involving electron sharing or exchange between functional groups on BRK and PO_4^{3-} ions. However, the reasonable fit of the pseudo-first-order theory indicates that physical adsorption also contributes to the overall process. Thus, the adsorption of PO_4^{3-} onto BRK likely involves a combination of both physisorption and chemisorption. This finding is consistent with the work of Ho [29], who studied second-order models for adsorption systems. However, this contrasts with findings related to the adsorption on biochar derived from peanut shell, which was found to be controlled by multiple processes of external and internal diffusion [30].

3.3. Analysis of adsorption thermodynamics

This study evaluated three thermodynamic parameters to understand the adsorption of PO_4^{3-} ions onto BRK: the standard Gibbs free energy change (ΔG, kJ/mol), the standard enthalpy change (ΔH, J/mol), and the standard entropy change (ΔS, kJ/(mol·K)). These parameters and Kd were calculated according to the equations reported in the literature [31, 32]. The calculated ΔG values were 724.54, 775.74, and 826.94 kJ/mol at temperatures of 10 °C, 30 °C, and 50 °C, respectively (Table 4).

A van't Hoff plot, created from the temperature-dependent data, showed a strong linear relationship with a coefficient of determination (R^2) of 0.95. This result validates the thermodynamic model used (Fig. 3). From the slope and intercept of the van't Hoff plot, the changes in enthalpy (ΔH) and entropy (ΔS) were determined. The negative entropy change (ΔS = -2.56 KJ/(mol·K)) indicates a reduction in randomness at the solid–liquid interface during the adsorption of PO_4^{3-} ions. This decrease is likely due to the structured arrangement of PO_4^{3-} on the BRK surface. The positive enthalpy change (ΔH = 22.67 J/mol) shows that the adsorption process is endothermic, requiring an energy input. The $\Delta H°$ values were primarily positive in studies that examined the adsorption thermodynamics of PO_4^{3-} onto adsorbents derived from biochar [18, 19, 33]. Across the studied temperature range, the Gibbs free energy change was positive ($\Delta G > 0$), showing that the adsorption of PO_4^{3-} onto BRK is thermodynamically non-spontaneous under the experimental conditions and is thermodynamically unfavourable. Overall, these findings suggest that the adsorption of PO_4^{3-} onto BRK is primarily driven by an endothermic physical interaction such as van der Waals forces, hydrogen bonding, or electrostatic attractions, rather than chemical bond formation. The interplay between the endothermic enthalpy and decreased entropy highlights the complex and non-spontaneous nature of this adsorption process, in which energy input is necessary to facilitate PO_4^{3-} uptake and induce ordering on the BRK surface.

Table 4. Thermodynamic parameters of PO_4^{3-} adsorption by BRK

Temperature (K)	K_d (L/mg)	LnK_d		ΔH (J/mol)	ΔS (KJ/mol·K)	ΔG (KJ/mol)
283	0.02222	-3.81	y= -2.727 – 307.93x	22.67	-2.56	724.54
303	0.02326	-3.76	R^2=0.95			775.74
323	0.02545	-3.67				826.94

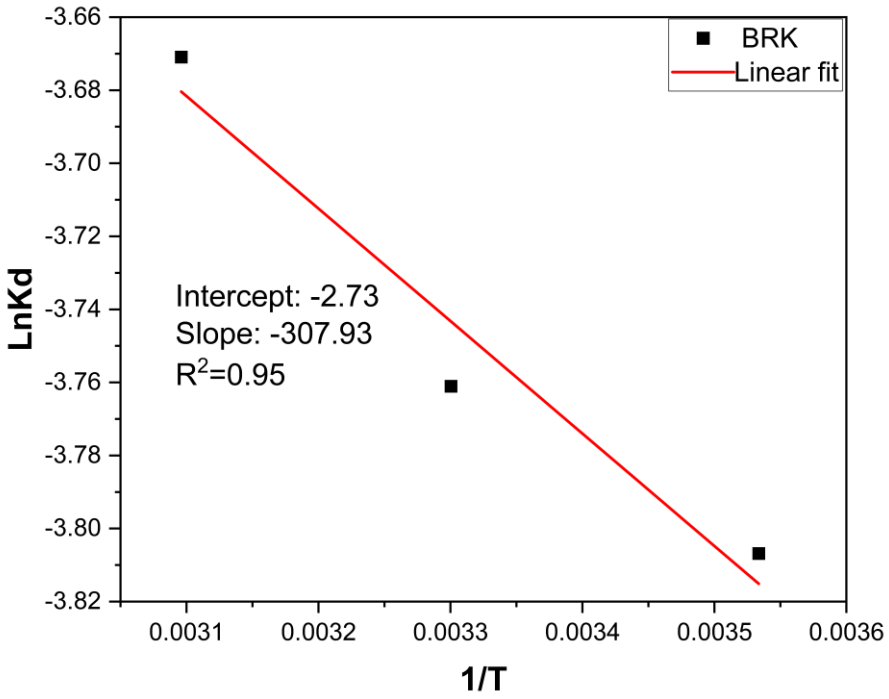

Fig. 3. Thermodynamics analysis of PO_4^{3-} adsorption by BRK

3.4. Effect of pH solution

The effect of pH on the adsorption efficiency and capacity of phosphatein solution is illustrated in Fig. 4. The results indicate a gradual rise in the adsorption capacity for phosphate as the pH rises from 1 to 7. However, the adsorption capacity declines sharply above pH 7. This phenomenon can be explained by the interaction between the different ionic forms of phosphate in solution and the adsorbent's surface charge characteristics.

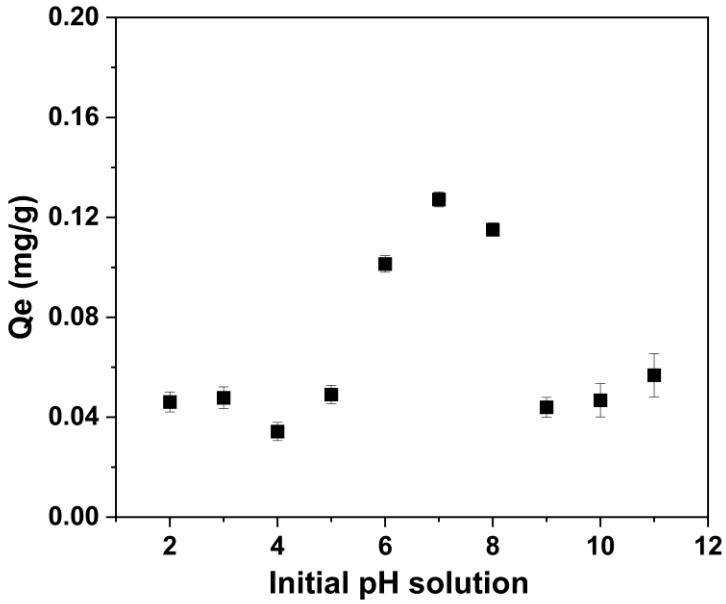

Fig. 4. Effect of pH on PO_4^{3-} adsorption capacity of BRK

Previous studies have shown that the BRK adsorbent used in this experiment has a point of zero charge (pH_{PZC}) of 9.1 [17]. Below this pH level of 9.1, the adsorbent surface carries a positive charge, favoring the adsorption of negatively charged phosphate species through electrostatic attraction [19]. Phosphate speciation also varies with pH. At strongly acidic pH (pH < 2), phosphate mainly exists as $H_3PO_4^-$. Under weak acidic conditions, particularly within the pH range of 2 to

4, phosphate predominantly exists as $H_2PO_4^-$. This particular form displays a notably lower affinity for the BRK adsorbent when compared to the other more prevalent phosphate speciation found in neutral or alkaline conditions. Consequently, this reduced affinity in acidic environments plays a crucial role in the significantly lower phosphate adsorption capacity found at pH 2–4, highlighting the intricate relationship between pH and adsorption efficiency.

At a neutral pH of 7, the positively charged BRK surface promotes strong electrostatic attraction toward the predominant phosphate speciation ($H_2PO_4^-$ and HPO_4^{2-}), resulting in the highest adsorption capacity. This favorable environment leads to an impressive adsorption capacity of 0.137 mg/g. When the solution pH exceeds 9.1, the adsorbent surface becomes negatively charged, leading to electrostatic repulsion with the negatively charged phosphate species. In addition, the increasing concentration of OH^- ions compete with phosphate for the available adsorption sites, further reducing the adsorption capacity under alkaline conditions.

3.5. Effect of co-existing anions

In this study, three common anions, including Cl^-, CO_3^{2-}, and SO_4^{2-}, were individually introduced into working solutions to evaluate their effects on the removal of PO_4^{3-} by BRK (Fig. 5). These anions were meticulously subjected at initial concentrations of 0.01 M and 0.1 M, allowing us to evaluate their competitive interactions with PO_4^{3-} ions in solution. The results revealed a marked decrease in PO_4^{3-} removal efficiency, highlighting the significant impact of these co-existing anions [34, 35].

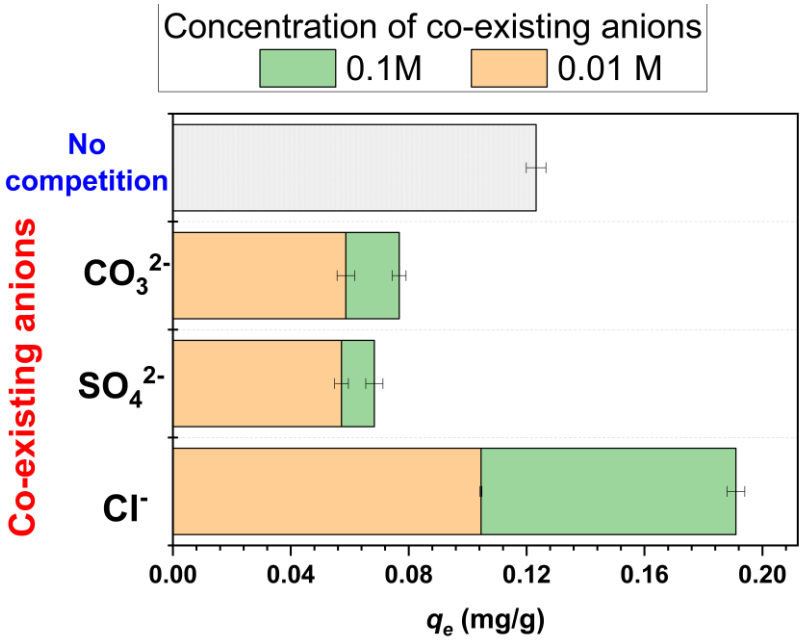

Fig. 5. Effect of coexisting anions on PO_4^{3-} adsorption capacity of BRK

As depicted in Fig. 6, an increase in the concentrations of these anions resulted in a pronounced decline in BRK's adsorption capacity for PO_4^{3-}. For instance, the presence of sulfate (SO_4^{2-}) at levels of 0.01 M and 0.1 M led to a dramatic reduction in PO_4^{3-} removal, dropping from 0.123 mg/g (when no competing anions were present) to 0.057 mg/g and 0.011 mg/g, respectively. A similarly striking decline was observed with carbonate ions: as their concentration rose from 0.01 M to 0.1 M, the removal capacity for PO_4^{3-} plummeted from 0.123 mg/g to 0.059 mg/g, and then further down to a mere 0.018 mg/g. This illustrates the formidable inhibitory effect of CO_3^{2-} on removal.

Throughout all tested concentrations, the competitive inhibition of co-existing anions for PO_4^{3-} ions followed a discernible hierarchy: no

competitor > Cl^- > CO_3^{2-} > SO_4^{2-}. This trend aligns with previous findings from [34], who also reported a similar competitive interaction among Cl^-, CO_3^{2-}, SO_4^{2-}, and NO_3^- to regarding the efficacy of Mg-Al layered double hydroxides in removing PO_4^{3-}. Specifically, the presence of CO_3^{2-} and SO_4^{2-} at a concentration of 300 mg/L resulted in a significant drop in PO_4^{3-} removal efficiency, from 90.82% to 53.98% and 74.54%, respectively. According to Gao et al. [35], the inhibitory effects of CO_3^{2-} and SO_4^{2-} can be attributed to their competitive adsorption of available sites and their influence on pH levels. Moreover, CO_3^{2-} can induce structural disruptions via ligand exchange, substantially hindering BRK's capacity to remove PO_4^{3-} ions. In contrast, Cl^- exerts a relatively minimal effect; it tends to form weaker outer-sphere complexes, thereby not competing intensely with PO_4^{3-} for adsorption sites.

3.6. Adsorbent characteristics

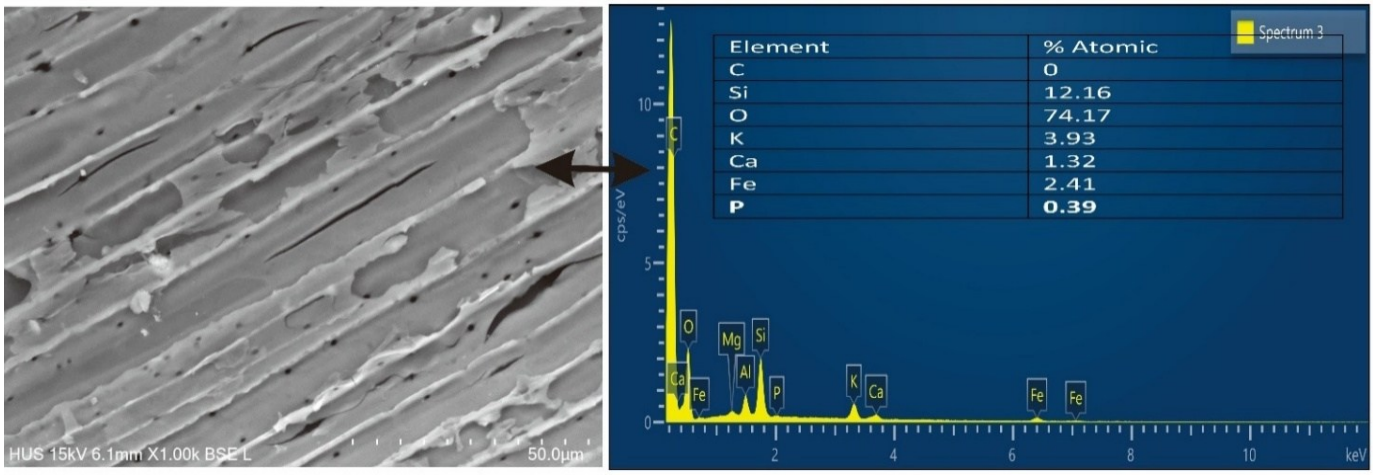

Fig. 6. SEM and EDX results of BRK

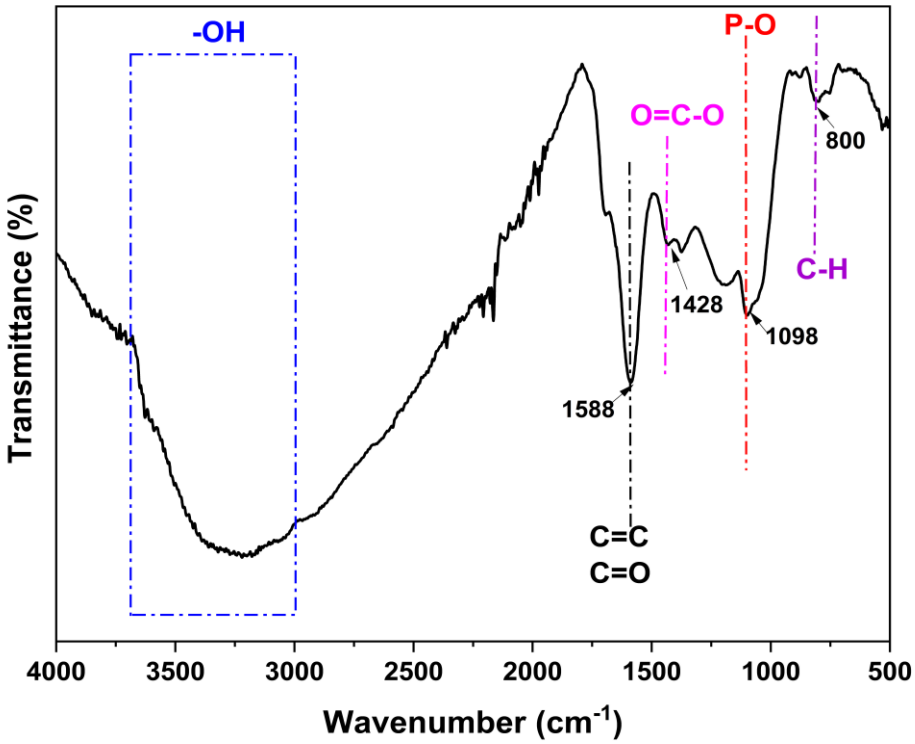

Fig. 7. FTIR spectra of BRK

Fig. 6 shows the SEM morphology of BRK and its elemental composition obtained by EDX after PO_4^{3-} adsorption. The characteristics of pristine BRK were previously reported [17] and are

briefly summarized in section 2.1. As seen in Fig. 6, BRK after PO_4^{3-} adsorption still exhibits a heterogeneous, porous surface with numerous voids and grooves of varying dimensions. This means that no significant changes in surface morphology after the adsorption process. The porous network remains intact, indicating that the adsorption process did not compromise the composite's structural integrity. However, EDX analysis shows the appearance of phosphorus, with its content increasing to 0.39%, suggesting successful adsorption of PO_4^{3-} ions onto the BRK surface (Fig. 6).

Fig. 7 presents the FTIR spectra of BRK after the PO_4^{3-} adsorption process. It can be observed that, following adsorption, the PO_4^{3-}-loaded BRK still exhibits four major characteristic bands, including –OH, C=O, C=C, and P-O, which are largely similar to the functional groups present in the pristine BRK. However, noticeable shifts in the vibrational bands occurred after adsorption. For example, the large band at 3245 cm^{-1}, attributed to the –OH stretching vibration in pristine BRK, shifted to 3219 cm^{-1} in the PO_4^{3-}-loaded BRK [17]. Similarly, the band at approximately 1622 cm^{-1}, characteristic of the C=O group in pristine BRK, shifted to 1598 cm^{-1} after the adsorption process [17].

Notably, the emergence of a peak at 1098 cm^{-1} is consistent with the P–O bond's vibrational mode, confirming the presence of P species on the BRK surface [36-38]. This demonstrates successful adsorption of PO_4^{3-} onto BRK.

3.7. Future perspectives

This study demonstrates that the bentonite–rice husk composite (BRK) is capable of adsorbing PO_4^{3-}, although its adsorption capacity is relatively lower than that of many previously reported adsorbents. However, when considered together with its excellent ammonium (NH_4^+) removal capacity, reaching up to 20.57 mg/g as reported in our previous study [17], these results indicate that BRK can effectively interact with both anionic and cationic pollutants. In aquatic environments, arsenate (AsO_4^{3-}) shares strong physicochemical similarities with PO_4^{3-}, including tetrahedral geometry, proton affinity, and comparable adsorption mechanisms, particularly a strong tendency to form inner-sphere complexes reaction [33, 39, 40]. As a result, adsorbents that are effective for PO_4^{3-} removal are therefore frequently found to also exhibit substantial AsO_4^{3-} adsorption, suggesting that BRK may have additional potential for AsO_4^{3-} remediation in contaminated water. This discussion further supports the conclusion that BRK can simultaneously remove multiple contaminants, highlighting its suitability for application in complex water treatment systems.

To further improve BRK's anion removal performance, future studies should explore targeted modifications, such as metal loading [10], to enhance adsorption efficiency toward anionic pollutants while preserving its high cation removal capacity. Overall, these findings support the development of BRK as a low-cost, and multifunctional material with potential for simultaneous removal of diverse pollutants from contaminated water.

4. Conclusions

Kinetic, equilibrium, thermodynamic, and effect of co- existing anions of material synthesized from bentonite and rice husk for the adsorption of PO_4^{3-} from water were investigated. The adsorption of PO_4^{3-} onto BRK likely involves a combination of both physisorption and chemisorption, based on the developed surface and electron sharing or exchange between functional groups on BRK and PO_4^{3-} ions. Langmuir model was best suited for explaining the adsorption isotherm of BRK, indicating that the adsorption mainly follows monolayer coverage on a homogeneous surface with a limited number of identical active sites, with a Langmuir maximum adsorption capacity reaching 1.37 mg/g for the adsorption process at 30 °C. pH had had a significant effect on the material's adsorption

performance with the optimal pH for the adsorption was 7. Among the tested anions, SO_4^{2-} had the most significant impact on PO_4^{3-} adsorption, likely due to structural interference via ligand exchange mechanisms. BRK is a sustainable, low-cost, multifunctional adsorbent capable of simultaneously removing multiple anionic and cationic contaminants from water, with further improvement through targeted modifications being necessary

References

[1] C. da Luz, S.M. de Arruda Guelli Ulson de Souza, A.A. Ulson de Souza, A. Dervanoski, A. de Oliveira Samel Moraes, B.D. Wood. (2018). A multiscale model for carbon adsorption of BTX compounds: Comparison of volume averaging theory and experimental measurements. *Chemical Engineering Science*, 184, 285-308. https://doi.org/10.1016/j.ces.2018.02.047

[2] K.S. Karthika, I. Rashmi, M.S. Parvathi. (2018). Biological Functions, Uptake and Transport of Essential Nutrients in Relation to Plant Growth. *Plant Nutrients and Abiotic Stress Tolerance*, 1-49. *Springer*. https://doi.org/10.1007/978-981-10-9044-8_1

[3] S.B. Kurniawan, A. Ahmad, M.F. Imron, S.R.S. Abdullah, A.R. Othman, H.A. Hasan. (2022). Potential of microalgae cultivation using nutrient-rich wastewater and harvesting performance by biocoagulants/bioflocculants: Mechanism, multi-conversion of biomass into valuable products, and future challenges. *Journal of Cleaner Production*, 365, 132806. https://doi.org/10.1016/j.jclepro.2022.132806

[4] K. Klein, A. Mandel, H. Lilleoja, S. Salmar, T. Tenno. (2020). Assessment of enhanced biological phosphorus removal process inhibition. *SN Applied Sciences*, 2, 1489. https://doi.org/10.1007/s42452-020-03281-1

[5] X. Xu, B. Wang, H. Tang, Z. Jin, Y. Mao, T. Huang. (2020). Removal of phosphate from wastewater by modified bentonite entrapped in Ca-alginate beads. *Journal of Environmental Management*, 260, 110130. https://doi.org/10.1016/j.jenvman.2020.110130

[6] T.E. Bektaş, B.K. Uğurluoğlu, B. Tan. (2021). Phosphate removal by Ion exchange in batch mode. *Water Practice & Technology*, 16(4), 1343-1354. https://doi.org/10.2166/wpt.2021.072

[7] K. Rajaniemi, T. Hu, E.-T. Nurmesniemi, S. Tuomikoski, U. Lassi. (2021). Phosphate and Ammonium Removal from Water through Electrochemical and Chemical Precipitation of Struvite. *Processes*, 9(1), 150. https://doi.org/10.3390/pr9010150

[8] E. Mohammadi, H. Daraei, R. Ghanbari, S.D. Athar, Y. Zandsalimi, A. Ziaee, A. Maleki, K. Yetilmezsoy. (2019). Synthesis of carboxylated chitosan modified with ferromagnetic nanoparticles for adsorptive removal of fluoride, nitrate, and phosphate anions from aqueous solutions. *Journal of Molecular Liquids*, 273, 116-124. https://doi.org/10.1016/j.molliq.2018.10.019

[9] D.T. Mekonnen, E. Alemayehu, B. Lennartz. (2021). Fixed-Bed Column Technique for the Removal of Phosphate from Water Using Leftover Coal. *Materials*, 14(19), 5466. https://doi.org/10.3390/ma14195466

[10] I.W. Almanassra, V. Kochkodan, G. Mckay, M.A. Atieh, T. Al-Ansari. (2021). Review of phosphate removal from water by carbonaceous sorbents. *Journal of Environmental Management*, 287, 112245. https://doi.org/10.1016/j.jenvman.2021.112245

[11] I. Kamika, M. Coetzee, B.B. Mamba, T. Msagati, M.N.B. Momba. (2014). The Impact of Microbial Ecology and Chemical Profile on the Enhanced Biological Phosphorus Removal (EBPR) Process: A Case Study of Northern Wastewater Treatment Works, Johannesburg. *International Journal of Environmental Research and Public Health*, 11(3), 2876-2898. https://doi.org/10.3390/ijerph110302876

[12] V. Vimonses, S. Lei, B. Jin, C.W.K. Chow, C. Saint. (2009). Kinetic study and equilibrium isotherm analysis of Congo Red adsorption by clay materials. *Chemical Engineering Journal*, 148(2-3), 354-364. https://doi.org/10.1016/j.cej.2008.09.009

[13] Z. Yang, O. Xiao, B. Chen, L. Zhang, H. Zhang, X. Niu, S. Zhou. (2013). Perchlorate adsorption from aqueous solution on inorganic-pillared bentonites. *Chemical Engineering Journal*, 223, 31-39. https://doi.org/10.1016/j.cej.2013.02.085

[14] R.R. Pawar, P. Gupta, Lalhmunsiama, H.C. Bajaj, S.-M. Lee. (2016). Al-intercalated acid activated bentonite beads for the removal of aqueous phosphate. *Science of The Total Environment*, 572, 1222-1230. https://doi.org/10.1016/j.scitotenv.2016.08.040

[15] M. Ahmad, A.U. Rajapaksha, J.E. Lim, M. Zhang, N. Bolan, D. Mohan, M. Vithanage, S.S. Lee, Y.S. Ok. (2014). Biochar as a sorbent for contaminant management in soil and water: A review. *Chemosphere*, 99, 19-33. https://doi.org/10.1016/j.chemosphere.2013.10.071

[16] B. Qiu, X. Tao, H. Wang, W. Li, X. Ding, H. Chu. (2021). Biochar as a low-cost adsorbent for aqueous heavy metal removal: A review. *Journal of Analytical and Applied Pyrolysis*, 155, 105081. https://doi.org/10.1016/j.jaap.2021.105081

[17] T. Hoang-Minh, N.T. Hai, D.T. Hieu, T.T. Hoai, B.V. Dong, L.V. Dung, N.T.H. Ha. (2025). Removal of ammonium from water by a KOH-treated bentonite biochar composite. *Colloid and Polymer Science*, 303, 81-94. https://doi.org/10.1007/s00396-024-05335-x

[18] X. Liu, F. Shen, X. Qi. (2019). Adsorption recovery of phosphate from aqueous solution by CaO-biochar composites prepared from eggshell and rice straw. *Science of The Total Environment*, 666, 694-702. https://doi.org/10.1016/j.scitotenv.2019.02.227

[19] Q. Yin, M. Liu, H. Ren. (2019). Biochar produced from the co-pyrolysis of sewage sludge and walnut shell for ammonium and phosphate adsorption from water. *Journal of Environmental Management*, 249, 109410. https://doi.org/10.1016/j.jenvman.2019.109410

[20] M. El Bouraie, A.A. Masoud. (2017). Adsorption of phosphate ions from aqueous solution by modified bentonite with magnesium hydroxide $Mg(OH)_2$. *Applied Clay Science*, 140, 157-164. https://doi.org/10.1016/j.clay.2017.01.021

[21] S. Kizito, H. Luo, S. Wu, Z. Ajmal, T. Lv, R. Dong. (2017). Phosphate recovery from liquid fraction of anaerobic digestate using four slow pyrolyzed biochars: Dynamics of adsorption, desorption and regeneration. *Journal of Environmental Management*, 201, 260-267. https://doi.org/10.1016/j.jenvman.2017.06.057

[22] C. Fang, T. Zhang, P. Li, R.-f. Jiang, Y.-c. Wang. (2014). Application of Magnesium Modified Corn Biochar for Phosphorus Removal and Recovery from Swine Wastewater. *International Journal of Environmental Research and Public Health*, 11(9), 9217-9237. https://doi.org/10.3390/ijerph110909217

[23] C. Fang, T. Zhang, P. Li, R. Jiang, S. Wu, H. Nie, Y. Wang. (2015). Phosphorus recovery from biogas fermentation liquid by Ca–Mg loaded biochar. *Journal of Environmental Sciences*, 29, 106-114. https://doi.org/10.1016/j.jes.2014.08.019

[24] W. Xiong, J. Tong, Z. Yang, G. Zeng, Y. Zhou, D. Wang, P. Song, R. Xu, C. Zhang, M. Cheng. (2017). Adsorption of phosphate from aqueous solution using iron-zirconium modified activated carbon nanofiber: Performance and mechanism. *Journal of Colloid and Interface Science*, 493, 17-23. https://doi.org/10.1016/j.jcis.2017.01.024

[25] L.-g. Yan, Y.-y. Xu, H.-q. Yu, X.-d. Xin, Q. Wei, B. Du. (2010). Adsorption of phosphate

from aqueous solution by hydroxy-aluminum, hydroxy-iron and hydroxy-iron–aluminum pillared bentonites. *Journal of Hazardous Materials*, 179(1-3), 244-250. https://doi.org/10.1016/j.jhazmat.2010.02.086

[26] H. Xi, F. Min, Z. Yao, J. Zhang. (2023). Facile fabrication of dolomite-doped biochar/bentonite for effective removal of phosphate from complex wastewaters. *Frontiers of Environmental Science & Engineering*, 17, 71. https://doi.org/10.1007/s11783-023-1671-7

[27] I. Perassi, L. Borgnino. (2014). Adsorption and surface precipitation of phosphate onto $CaCO_3$–montmorillonite: effect of pH, ionic strength and competition with humic acid. *Geoderma*, 232-234, 600-608. https://doi.org/10.1016/j.geoderma.2014.06.017

[28] I.W. Almanassra, G. Mckay, V. Kochkodan, M. Ali Atieh, T. Al-Ansari. (2021). A state of the art review on phosphate removal from water by biochars. *Chemical Engineering Journal*, 409, 128211. https://doi.org/10.1016/j.cej.2020.128211

[29] Y.-S. Ho. (2006). Review of second-order models for adsorption systems. *Journal of Hazardous Materials*, 136(3), 681-689. https://doi.org/10.1016/j.jhazmat.2005.12.043

[30] K.-W. Jung, M.-J. Hwang, K.-H. Ahn, Y.-S. Ok. (2015). Kinetic study on phosphate removal from aqueous solution by biochar derived from peanut shell as renewable adsorptive media. *International Journal of Environmental Science and Technology*, 12, 3363-3372. https://doi.org/10.1007/s13762-015-0766-5

[31] Z. Guo, X. Liu, H. Huang, L. Jiang. (2017). Adsorption thermodynamics and kinetics of yohimbine onto strong acid cation exchange fiber. *Journal of the Taiwan Institute of Chemical Engineers*, 71, 1-12. https://doi.org/10.1016/j.jtice.2016.05.012

[32] D. Guimarães, V.A. Leão. (2014). Batch and fixed-bed assessment of sulphate removal by the weak base ion exchange resin Amberlyst A21. *Journal of Hazardous Materials*, 280, 209-215. https://doi.org/10.1016/j.jhazmat.2014.07.071

[33] N. Zhu, T. Yan, J. Qiao, H. Cao. (2016). Adsorption of arsenic, phosphorus and chromium by bismuth impregnated biochar: Adsorption mechanism and depleted adsorbent utilization. *Chemosphere*, 164, 32-40. https://doi.org/10.1016/j.chemosphere.2016.08.036

[34] Y. Huang, X. Fan, H. Wang, Z. Li, D. Xiong, Y. Pei. (2023). Tuning Mg-Al layered double hydroxides synthesized from the novel ionic liquid-based surfactant-free microemulsion for efficiently phosphate removal in aqueous solutions. *Journal of Molecular Liquids*, 382, 121826. https://doi.org/10.1016/j.molliq.2023.121826

[35] D. Gao, W. Zhang, H. Dong, Y. Yu, W. Liu, H. Luo, Z. Jing, B. Liang, L. Peng, B. Wu, T. Huang, H. Cheng. (2025). Phosphorus removal from water by the layered double hydroxides (LDHs)-based adsorbents: A review for structure, mechanism, and current progress. *Environmental Technology & Innovation*, 37, 104003. https://doi.org/10.1016/j.eti.2024.104003

[36] Y. Qin, X. Wu, Q. Huang, J. Beiyuan, J. Wang, J. Liu, W. Yuan, C. Nie, H. Wang. (2023). Phosphate Removal Mechanisms in Aqueous Solutions by Three Different Fe-Modified Biochars. *International Journal of Environmental Research and Public Health*, 20(1), 326. https://doi.org/10.3390/ijerph20010326

[37] P. Tu, G. Zhang, Y. Cen, B. Huang, J. Li, Y. Li, L. Deng, H. Yuan. (2023). Enhanced phosphate adsorption and desorption characteristics of MgO-modified biochars prepared via direct co-pyrolysis of MgO and raw materials. *Bioresources and*

Bioprocessing, 10, 49. https://doi.org/10.1186/s40643-023-00670-3

[38] J. Guo, H. Xiao, J.B. Zhang, C. Dai, T. Li, M.-t. Gao, J. Hu, J. Li. (2024). Characterization of highly stable biochar and its application for removal of phenol. *Biomass Conversion and Biorefinery*, 14(12), 13311-13321. DOI 10.1007/s13399-022-03375-3

[39] Y. Huang, J.-K. Yang, A.A. Keller. (2014). Removal of Arsenic and Phosphate from Aqueous Solution by Metal (Hydr-)oxide Coated Sand. *ACS Sustainable Chemistry & Engineering*, 2(5), 1128-1138. https://doi.org/10.1021/sc400484s

[40] L.N. Pincus, P.V. Petrović, I.S. Gonzalez, E. Stavitski, Z.S. Fishman, H.E. Rudel, P.T. Anastas, J.B. Zimmerman. (2021). Selective adsorption of arsenic over phosphate by transition metal cross-linked chitosan. *Chemical Engineering Journal*, 412, 128582. https://doi.org/10.1016/j.cej.2021.128582